Applied Catalysis B: Environmental 125 (2012) 507–515

Contents lists available at SciVerse ScienceDirect

Applied Catalysis B: Environmental

journal homepage: www.elsevier.com/locate/apcatb

Gold catalysts for low temperature water-gas shift reaction: Effect of ZrO_2 addition to CeO_2 support

Floriana Vindigni[a], Maela Manzoli[a], Tatyana Tabakova[b], Vasko Idakiev[b], Flora Boccuzzi[a], Anna Chiorino[a,*]

[a] Department of Chemistry and NIS Centre of Excellence, University of Torino, via P. Giuria 7, 10125 Torino, Italy
[b] Institute of Catalysis, Bulgarian Academy of Sciences, Acad. G. Bonchev Str., bl. 11, 1113 Sofia, Bulgaria

ARTICLE INFO

Article history:
Received 14 March 2012
Received in revised form 18 May 2012
Accepted 24 May 2012
Available online 1 June 2012

Keywords:
WGSR
Highly dispersed gold
Ceria
Zirconia
CeO_2–ZrO_2 mixed phase
Acid/base properties
FTIR

ABSTRACT

New gold catalysts supported on ceria modified by addition of ZrO_2 have been synthesized and tested in the water-gas shift reaction (WGSR) at low temperature, where they displayed better catalytic activity than gold supported on pure ceria, following the trend: AuCe50Zr50 > AuCe80Zr20 > AuCe. Morphologic, textural, structural and spectroscopic characterisation showed that the addition of zirconia to ceria leads to the formation of mixture of tetragonal ceria–zirconia phases. Moreover, depending on the zirconia amount, a different Au dispersion is observed. Au agglomerates (10–20 nm) and nanoparticles (about 2.5 nm) have been detected by HRTEM on AuCe80Zr20, while only nanoparticles have been found on AuCe50Zr50. FTIR spectroscopy of CO adsorbed at 120 K showed also the presence of Au clusters, more abundant on AuCe50Zr50 than on AuCe80Zr20. However, at low temperature the best catalytic activity of AuCe50Zr50 is correlated not only to the abundance of gold clusters and nanoparticles, but also to the effect of ZrO_2 addition that influences the acid/base surface properties of ceria, as successfully demonstrated by adsorption and surface reaction of acetone vapor at room temperature. FTIR measurements performed before and after reaction showed that the carbonate-like species have the lowest stability on the AuCe50Zr50 surface. This feature, along with the presence of a high gold dispersion, makes AuCe50Zr50 the best catalyst in terms of activity and stability.

1. Introduction

Traditionally hydrocarbons (oil or natural gas) have been the hydrogen source, although in the future the exploitation of some renewable materials, such as biomass, or waste recycling is expected. In technological terms the main challenges arise during the initial conversion of the source material into a "synthesis gas" mixture comprising carbon monoxide, carbon dioxide, hydrogen and water. The high concentration of carbon monoxide, as well of the desired high purity hydrogen, makes an additional purification of the synthesis gas essential when it is intended for feeding the PEMFC: as carbon monoxide poisons the electrodes in the PEMFC, it is necessary to obtain residual carbon monoxide levels typically below 50 ppm. The WGSR is usually involved in the preliminary CO abatement from the "synthesis gas", hopefully carried out at low temperature. In the past 10 years it has been discovered that oxide-supported gold catalysts can have a remarkably high activity for the WGS reaction at low temperature providing that the materials are prepared in proper ways. There has been much debate in the literature with regard to the activity and stability of supported gold catalysts variously prepared or activated. The method of preparation and pre-treatment [1] of the gold catalysts is critical and activity changes of several orders of magnitude can be observed depending on the methods chosen. It has been shown that an intimate contact between gold and the oxide support is important and any preparative procedure that does not generate such an interaction, or any subsequent treatment that can destroy such an interaction, may result in catalysts with low activity. It is generally accepted that the nature of the support plays a decisive role on the dispersion and shape of gold particles, that is reflected directly on the catalytic activity. The effect of support on the reactivity of gold-based catalysts has been commented recently by Chen and Goodman [2].

Many evidences have been found that Au supported on different metal oxides shows significant WGS activity [3–17] Moreover, systems based on ceria have been considered with attention, as also Au/CeO_2 [18–30] has been found to perform very well in the WGSR.

The success of ceria in several catalytic applications is mainly due to its characteristic feature, the ability to shift easily between oxidized and reduced state ($Ce^{4+} \leftrightarrow Ce^{3+}$) [31], giving its unique oxygen storage capacity (OSC). This OCS, strictly connected to

* Corresponding author.
E-mail address: anna.chiorino@unito.it (A. Chiorino).

0926-3373/$ – see front matter © 2012 Elsevier B.V. All rights reserved.
http://dx.doi.org/10.1016/j.apcatb.2012.05.031

high oxygen defectivity, makes CeO_2 an appropriate support for precious metals, promoting noble metal activity and dispersion [32]. In fact, oxygen vacancies, that are the most relevant surface defects, play a crucial role for binding catalytically active species: when Au nanoparticles are supported on ceria, the system exhibits a high activity for the WGS reaction over a wide temperature range [33]. Despite that, pure cerium dioxide is poorly thermostable as it undergoes sintering at high temperature, thereby losing its crucial oxygen storage and release ability [34,35]. In addition, all known WGS catalysts based on ceria show similar problems related to the deactivation with time-on-stream and/or shut-down restart operation. For example, Kim and Thompson [36] reported fast deactivation of their Au–ceria catalyst, which was attributed to the blockage of the active sites by carbonates and/or formates formed during the WGS reaction. They reported that the oxygen deficiency is an important factor with regard to the formation of carbonate and formate species on oxide surface. It was also found that the initial activities for the Au/CeO_2 catalysts could be fully recovered by calcination of the deactivated catalysts in flowing air at elevated temperatures. Since the deposition of carbonates and/or formates was facilitated by oxygen-deficient sites on the catalyst surface, they proposed that deactivation could be influenced by the addition of constituents, as ZrO_2, to control oxygen deficiency and decrease the formation of carbonates species [37]. It was previously reported that the incorporation of ZrO_2 into a solid solution with CeO_2 has a significant effect on both OSC and stability of this defective oxide [33,38]. In particular, the Zr presence, unlike on pure ceria, allows the storage and release of oxygen also from the bulk lattice structure and not just from surface layers. However, ZrO_2 addiction gives rise to a modification of support surface and, as a consequence, could also affect the gold dispersion. Tibiletti et al. in a DFT and in situ EXAFS study on $Au/CeZrO_4$ catalyst evidenced that the presence of zirconium in the oxide support stabilizes the oxygen defects surrounding the gold particles [39]. These defects are critical in the reaction mechanism and promote the WGS activity. Later, some of the same authors reported that the catalysts deactivation was due to the detachment of the gold particles from the $CeZrO_4$ support in the presence of water [40]. This is due to the hydrolysis of the interface between the gold and the oxide that decreases the metal support interaction by a breakage of the Au-support link at the metal-oxide interface.

In this paper the catalytic activity in the WGS reaction of new gold catalysts supported on ceria, modified with the addition of ZrO_2 is presented. In particular, we will focus on the results obtained at low temperature. Morphologic, textural and spectroscopic analysis has been undertaken in order to examine the impact of zirconia addition to CeO_2 and to explain the catalytic trend displayed below 500 K. In particular, HRTEM and BET measurements were performed to investigate the effect of the Zr presence on both ceria texture and Au dispersion. In order to have information on the surface sites distribution, FTIR studies have been done at 120 K on the catalyst before and after the water-gas shift reaction, using CO as probe molecule. The results have been presented together with a careful comparison with Au supported on bare CeO_2 to understand if the addition of ZrO_2 can improve the catalytic activity and decrease the deactivation. Finally, to evaluate the surface acid/base properties of the samples, FTIR spectra of adsorbed acetone on oxidized supports have been undertaken and analyzed.

2. Experimental

2.1. Catalyst preparation

The syntheses of the supports and of the gold catalysts were carried out in a "Contalab" laboratory reactor enabling complete control of the reaction parameters (pH, temperature, stirrer speed, reactant feed flow, etc.) and high reproducibility.

Pure ceria and zirconia supports were prepared by precipitation of $Ce(NO_3)_3{\cdot}6H_2O$ or $ZrCl_4$ with K_2CO_3 at pH 9.0 and at 333 and 353 K, respectively; the precipitates were dried and calcined in air at 673 K for pure ceria, at 773 K for pure zirconia.

The mixed CeO_2–ZrO_2 supports (80:20 and 50:50 ratios as wt.%) were obtained by coprecipitation method (CP). Mixed aqueous solutions of $Ce(NO_3)_3$, $ZrCl_4$ and precipitant K_2CO_3 reacted under vigorous stirring at constant pH 9.0 and temperature 353 K. The resulting precipitates were aged at the same temperature for 2 h (h), then filtered and washed until removal of NO_3^- and Cl^- ions. After washing the precipitates were dried in vacuum at 353 K and calcined under air at 673 K for 2 h.

All catalysts were prepared by the deposition–precipitation method (DP) of gold on mixed supports suspended in water, via interaction of $HAuCl_4{\cdot}3H_2O$ and K_2CO_3 at a constant pH 7.0 and at a temperature of 333 K. After aging for 1 h, the precipitates were washed, dried in vacuum at 353 K, and calcined under air at 673 K for 2 h. The gold loading for each catalyst was 3 wt%. The catalysts were referred to AuCe, when pure ceria was used as support and to AuCe80Zr20 and AuCe50Zr50 in the case of Ce–Zr mixed supports with CeO_2:ZrO_2 ratio 80:20 and 50:50, respectively. An Au/ZrO_2 (AuZr) sample prepared in the same way was used as comparison for structural characterisation.

2.2. Characterisation techniques

Specific surface areas of the powders were determined by N_2 adsorption at 77 K (BET method) with a Micromeritics ASAP 2100 apparatus on the oxides outgassed at 423 K.

X-ray powder diffraction (XRPD) patterns were collected with a PW3050/60 X'Pert PRO MPD diffractometer from PANalytical working in Bragg–Brentano geometry, using as a source the high-powered ceramic tube PW3373/10 LFF with a Cu anode ($\lambda = 0.541$ Å) equipped with a Ni filter to attenuate K_β. Scattered photons have been collected by a real time multiple strip (RTMS) X'celerator detector. A suspension of the powdered samples has been deposited onto a silicon plate mounted on a rotating goniometer head. Data were collected in the $10 \leq 2\theta \leq 100^\circ$ angular range, with 0.02° 2θ steps. The samples were examined in their as-received form.

High-resolution transmission electron microscopic (HRTEM) analysis has been performed by means of a JEOL JEM 3010-UHR microscope operating at 300 kV, equipped with a $(2k \times 2k)$-pixel Gatan US1000 CCD camera and with an OXFORD INCA EDS instrument for atomic recognition via energy dispersive spectroscopy (EDS). The powdered samples were deposited on a copper grid covered with a lacey carbon film.

FTIR spectra were taken on a PerkinElmer 1760 spectrometer (equipped with a MCT detector) with the samples in self supporting pellets introduced in cells allowing thermal treatments in controlled atmospheres and spectrum scanning at room temperature (r.t.) or at controlled temperatures (from 120 to 300 K) in vacuum or in reduced pressure of probe gases. From each spectrum, the spectrum of the sample before the inlet of the probe was subtracted. The spectra were normalized respect to the gold content of each sample. Band integration was carried out by "Curvefit", in Spectra Calc (Galactic Industries Co.) by means of Lorentzian curves. FTIR analysis were undertaken on the catalysts previously submitted to a thermal treatment in O_2 at 473 K to clean the surface of the catalysts, which is covered of water and carbonate-like species because of the air exposure. After oxidation, the samples were heated from r.t. to 373 K in H_2, to mimic the same pretreatment to which the catalysts underwent before the WGS catalytic tests. These pre-activated catalysts will be denoted as "fresh" catalysts.

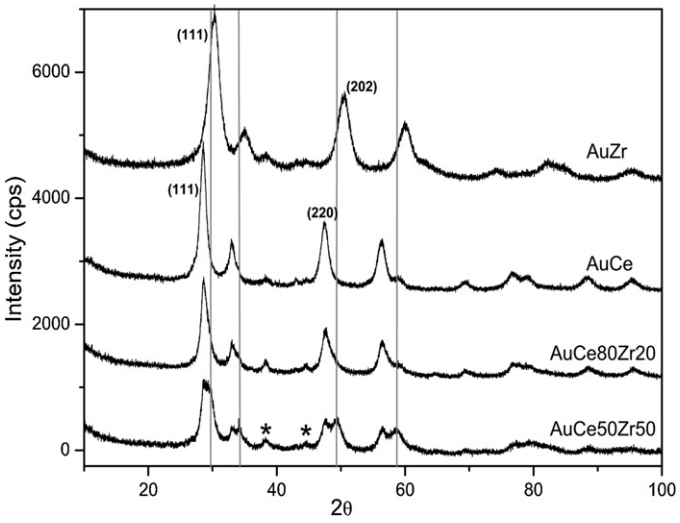

Fig. 1. XRPD patterns of AuCe50Zr50, AuCe80Zr20, AuCe and AuZr. The main peaks are indexed for AuCe and AuZr and highlighted with bars for AuCe50Zr50. The black stars indicate the diffraction peaks of Au nanoparticles.

With the aim to evaluate the effect of the reaction on the active surface sites, the FTIR measurements have been undertaken before and after the WGS reaction using CO as probe molecule at 120 K.

2.3. Catalytic activity measurements

WGS reaction activity measurements were carried out in a flow reactor at atmospheric pressure and temperature range from 413 to 623 K. Reactant gas mixture fed into the reactor contained 4.42 vol.% CO, the rest being argon. The following conditions were applied: catalyst bed volume = 0.5 cm^3 (0.63–0.80 mm pellets), space velocity = 4000 h^{-1}, partial pressure of water vapor = 31.1 kPa. The samples were previously subjected to a reduction treatment at 383 K for 1 h in a 1% H_2/Ar mixture. The analysis of the mixture converted at the reactor outlet was carried out on an "URAS-3G" (Hartmann & Braun AG) gas analyzer with respect to the CO content at steady-state conditions. Moreover, in order to test the stability, two cycles of WGS reaction were performed on AuCe50Zr50 sample.

3. Results and discussion

3.1. Textural, structural and morphological properties

Specific surface areas measurements were performed on all bare supports by N_2 adsorption at 77 K (Brunauer–Emmett–Teller) method. A specific surface area of 88 m^2/g was obtained for ceria, while the values measured for CeZr (80:20) and for CeZr (50:50) were 114 m^2/g and 112 m^2/g, respectively. These findings indicate that there is an increase on the surface area of the mixed oxide when zirconia is added to ceria by coprecipitation method. In Fig. 1 the X-ray powder diffraction patterns of AuCe80Zr20 and of AuCe50Zr50 are shown. The patterns related to AuCe and AuZr are also reported for comparison.

For the sake of clarity, the two main peaks of AuCe and AuZr are indexed. More in detail, AuCe shows two main features at 28.53 (2θ) and at 47.51 (2θ) that are indexed as (1 1 1) and (2 2 0) planes, respectively in the cubic-fluorite type structure (JCPDS file number: 034-0394). AuZr clearly shows the XRPD pattern of zirconium oxide in the tetragonal phase (JCPDS file number: 017-0932) where the peaks at 30.31 (2θ) and 50.49 (2θ) are attributed to (1 1 1) and (2 0 2) planes. The absence of the peaks related to tetragonal zirconia is firstly observed in both XRPD patterns of AuCe80Zr20 and of AuCe50Zr50.

At the same time, the diffraction pattern of AuCe50Zr50 is different from that related to AuCe. In particular, four new peaks, highlighted with bars, at 29.32 (2θ), 34.15 (2θ), 49.31 (2θ) and 58.65 (2θ) are present. These features can correspond to tetragonal mixed phases, whose existence is reported in literature at intermediate compositions of CeO_2–ZrO_2 systems (20–80 mol%) [41,42].

The diffraction pattern of AuCe80Zr20 is apparently similar to that of AuCe, indicating that CeO_2 in the cubic-fluorite type structure is the predominant phase. However, an asymmetric broadening of the peaks (particularly evident in those at 2θ equal to 33.02 and 47.51) is observed. This feature, in addition to the absence of the peaks related to tetragonal zirconia, can be an indication that also in this case a mixture of tetragonal solid solutions is present, randomly distributed throughout the ceria phase. Finally, two diffraction peaks were observed at 38.30 (2θ) and 44.50 (2θ), corresponding to Au (1 1 1) and Au (2 0 0), evidenced by the black stars only on AuCe50Zr50 pattern for convenience.

HRTEM analysis of the AuCe sample was performed previously [43]. Briefly, big Au agglomerates with size of at least 10 nm and very highly dispersed clusters with size of about 1 nm, whose presence was confirmed by EDS, were observed on this catalyst, together with ceria nanoparticles with average size of 4.5 nm. The HRTEM measurements performed on the AuCe80Zr20 sample revealed that no zirconia particles exist as separate phase, while mainly crystalline ceria particles with size comparable with that observed for AuCe have been detected. These last results are in agreement with XRPD findings. Moreover, HRTEM analysis pointed out that big gold particles, with size ranging between 10 and 15 nm, are present on AuCe80Zr20, as shown in Fig. 2 (section a).

The distance between the diffraction fringes of these particles indicates that gold is in its metallic form (section b). In addition, also Au nanoparticles, having average size around 2.5 nm, have been observed on the same sample (section c, for the sake of clarity Au nanoparticles are indicated by arrows). The above findings clearly evidenced that AuCe80Zr20 has a bimodal gold particle size distribution (reported in section d).

Quite different observations were collected when performing HRTEM measurements on AuCe50Zr50. Firstly, the mixed oxide support looks quite different from that of AuCe80Zr20. No zones with different phase and morphology contrast were detected and EDS mapping evidenced that Ce and Zr are quite uniformly dispersed on the sample, as shown in Fig. 3 (section a). These results are in agreement with the presence of a mixture of tetragonal solid solutions, as previously shown by XRPD data. Despite that the formation of a thermodynamically stable solid solution is not favored over the whole range of compositions, it was reported [44] that an homogeneous distribution of the Ce and Zr cations in the lattice of the mixed oxides, with negligible local enrichments in one or the other phase, makes difficult the phase segregation process, improving the solid solution stability.

Moreover, a quite contrasting Au dispersion is also observed on the AuCe50Zr50 sample, since only very small nanoparticles with roundish shape and homogeneous in size have been observed (see section b of Fig. 3, where the Au nanoparticles have been evidenced by arrows). The particle size distribution (reported in section c) is narrow and the obtained average diameter is 1.55 ± 0.30 nm.

3.2. Catalytic activity

The main goal of the present research work is devoted to the development of WGS catalysts with improved activity and stability at low temperature. The equilibrium conversion of CO is largely

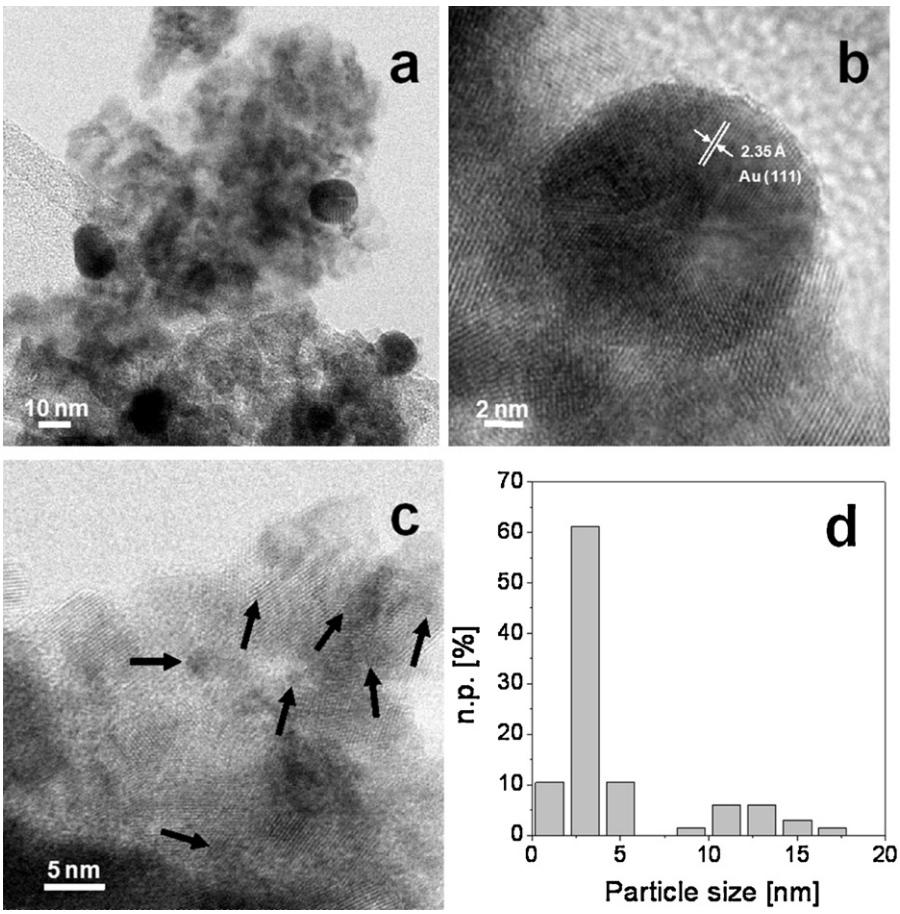

Fig. 2. Low magnification TEM image of AuCe80Zr20 (section a). HRTEM details in which a big Au particle is shown (section b) together with very small Au particles (section c) and relative particle size distribution (section d). Instrumental magnification: 150,000×, 800,000×, 500,000×.

dependent on the reaction temperature: since WGSR is an exothermic reaction, at lower temperature a higher CO removal can be favored. On the other hand, from the viewpoint of kinetics, the reactant gases are not active enough to reach the chemical equilibrium at low temperatures. For this reason the design of more active low-temperature shift catalysts will allow the conversion to approach the equilibrium limit more closely. On this premise, the attention will be mainly focussed on catalytic performance in the temperature range below 500 K. The temperature dependence of the CO conversion during the WGS reaction over the gold catalysts supported on mixed CeO_2–ZrO_2, as well on pure CeO_2, is shown in Fig. 4.

First of all, the comparison between the catalytic behavior of the catalysts clearly shows that the addition of ZrO_2 influences the catalytic performance, giving rise to an increase in the CO conversion at low temperature, particularly evident around 450 K.

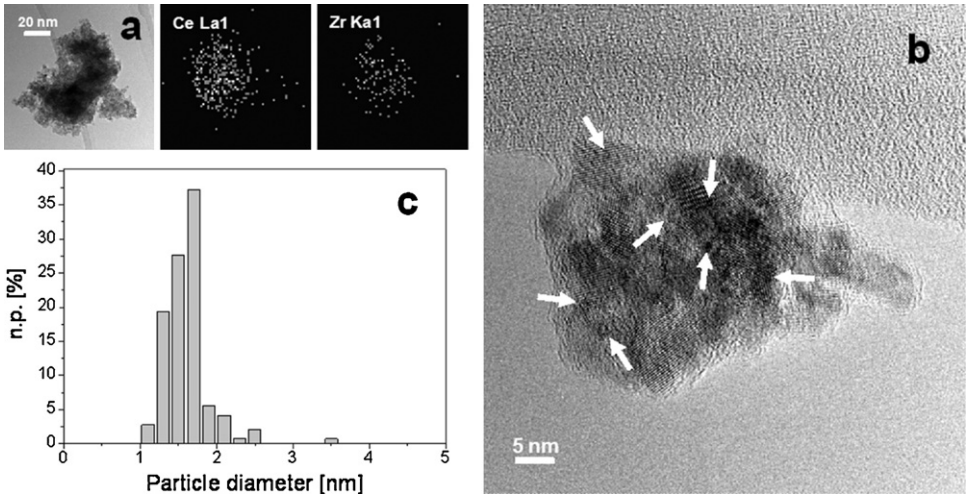

Fig. 3. Low magnification TEM micrograph image representing sample of AuCe50Zr50 with EDS maps of the same region, allowing speciation of Ce and Zr elements to be done (section a). HRTEM image of AuCe50Zr50 (section b) and gold particle size distribution (section c). Instrumental magnification: 60,000× and 300,000×, respectively.

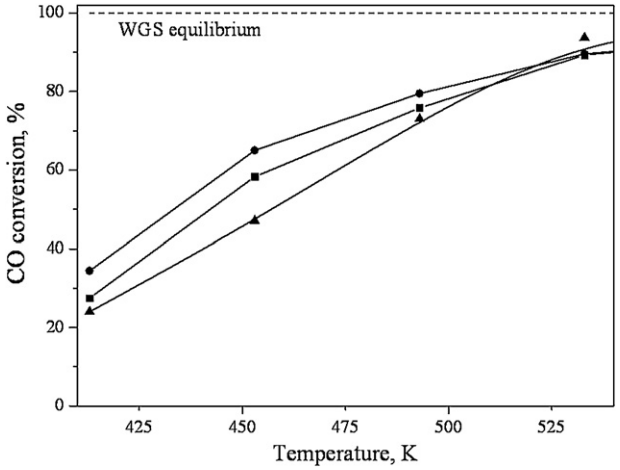

Fig. 4. Catalytic activity in WGS reaction of AuCe (▲) AuCe80Zr20 (■) and AuCe50Zr50 (●).

Moreover, the observed increase is closely related to the amount of added zirconia: namely, the catalyst with the higher ZrO_2 loading (i.e. AuCe50Zr50) is the most active in the WGS reaction in the temperature range below 500 K. All studied catalysts demonstrate very similar activities above 525 K.

In order to test the stability, the catalytic run was further repeated on AuCe50Zr50, i.e. the sample with the best performance. The comparison between the two cycles is reported in Fig. 5.

More in detail, the first cycle was performed adopting the experimental conditions described in Section 2.2, and denoted as I run (Fig. 5, black line). Then the reactor was cooled to r.t. in the presence of the reaction mixture (CO, water, CO_2, H_2, Ar) and kept at these conditions for 10 h. The test was repeated the next day and the results are denoted as II run (Fig. 5, grey line). In many cases the conclusion for the stability is drawn on the basis of catalytic tests performed at a given temperature for a certain period of time. However, in order to have more detailed information for the catalytic behavior in the whole temperature interval, we measured stationary CO conversion within 2 h after attainment of steady-state conditions at a given temperature. Stable CO conversions were registered at each temperature, indicated in Fig. 5. The data obtained during the first and the second run are almost coincident at $T \geq 475$ K, indicating a substantial stability of the catalyst and lack of deactivation.

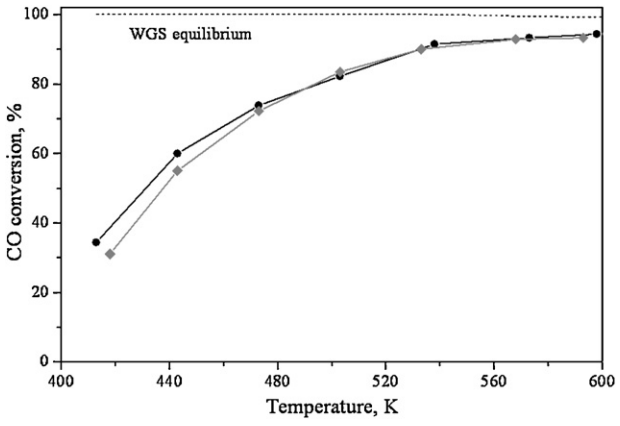

Fig. 5. Comparison between the first catalytic cycle (I run, black line) and the second one (II run, grey line) to which AuCe50Zr50 has been undergone.

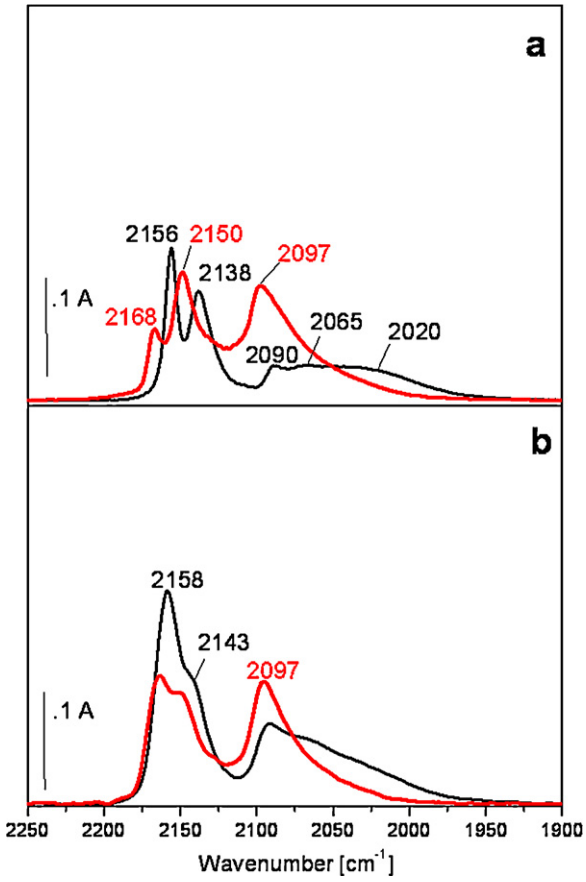

Fig. 6. FTIR spectra of CO adsorbed at 90 K on fresh AuCe (section a) and AuCe50Zr50 (section b), before (black curves) and after (red curves) WGS reaction.

3.3. FTIR characterization of the exposed sites

3.3.1. CO adsorption at 120 K on the fresh catalysts

All samples have been characterized using CO as probe molecule at 120 K. Working at low temperature allows to have evidence of all surface sites, including those weakly interacting with the probe and not detectable at r.t. The FTIR absorption spectra collected on the fresh catalysts before the WGS reaction (black lines) are reported in Fig. 6 in the carbonylic stretching region. They are normalized respect to the gold content.

In the higher frequency side, CO adsorption on fresh AuCe (section a, black line) produced two bands centered at 2156 cm^{-1} and at 2138 cm^{-1}. The former is attributed to the stretching mode of the CO molecules adsorbed on Ce^{4+} support sites. The 2138 cm^{-1} peak is related to the adsorption of CO on Ce^{3+} sites [45], generated on the support surface by the reduction of uncoordinated Ce^{4+} sites due to the thermal treatment to which the sample has been previously submitted. On the contrary, on AuCe50Zr50 (section b, black line) a less resolved absorption centered at 2158 cm^{-1} with a shoulder at 2143 cm^{-1}, is evident in the higher frequency range. The shoulder in the low frequency side can be attributed to a liquid-like adsorbed CO phase [45]. Daturi et al. [46] have observed the same features in a mixed ceria–zirconia (50:50) sample, explaining their results as an evidence of a presence of a true solid solution. Particularly, the authors have highlighted that in a solid solution CO molecules adsorbed on Ce^{4+} sites are affected not only by the electrostatic field generated by the sites, but they are also sensitive to the neighboring Zr^{4+} sites. The result of these interactions is a broad band with unresolved component, centered at about 2165 cm^{-1}. On this basis, the band at 2158 cm^{-1} (Fig. 6, section b, black line) is assigned to CO

in interaction with the solid solution sites (either Zr^{4+} or Ce^{3+}). The FTIR results on AuCe50Zr50 support the presence of a solid solution and are in agreement with the XRD data (Fig. 1).

A broad and complex absorption extending from 2100 to 2000 cm^{-1} is observed in the spectrum of AuCe (Fig. 6, black line in section a). The 2100–2000 cm^{-1} is the typical range of the stretching vibration mode of CO adsorbed on Au sites. The position and the shape of the related band can show a wide variability, depending on the nature of active gold: metallic gold nanoparticles [47] and anionic [48] Au clusters have been proposed and widely discussed in many research works. The active form, that has effect on the catalyst activity, is strictly connected to the nature of the support. In our recent paper [49], we have reported FTIR analysis of adsorbed CO and of its isotopic mixtures on a series of gold catalysts, highlighting that the oxide on which the gold is deposited manages the nature, the structure and the oxidation state of the gold species.

The broad absorption observed on AuCe has a component at 2090 cm^{-1}, that can be assigned to CO adsorbed on flattened, thin gold particles present at the surface of defective ceria [43]. This flattening effect was also observed by Akita et al. during TEM observation [50]. The authors have associated the structural change of the Au particle to the reduction of CeO_2 support, evidenced by the electron energy loss spectroscopy (EELS) measurements, that is also an important issue under electron beam irradiation. Looking at the low frequency range, the components in the 2080–2020 cm^{-1} have been assigned [51] to negatively charged clusters, stabilized by the interaction with surface defects as oxygen vacancies and Ce^{3+}. Interestingly, the spectrum of AuCe50Zr50 (section b, black line) shows quite similar features, but with different relative abundance of the two main adsorbing gold species, i.e. nanoparticles and clusters, indicating that there is an effect of the support composition on gold dispersion. Finally, a band at 2098 cm^{-1}, related to CO adsorbed on Au° sites exposed at the surface of the nanoparticles, with a broad and weak tail at lower frequencies, due to CO adsorbed on Au clusters, has been observed in the case of AuCe80Zr20 (see Supporting information). In particular, the band at 2098 cm^{-1} is quite more intense than the broad component at lower frequency, indicating the presence of more nanoparticles than clusters on AuCe80Zr20, in agreement with the HRTEM results.

In order to quantify the amount of the uncoordinated Au sites, an integration of the carbonilyc bands observed in the 2100–2000 cm^{-1} range was carried out. Moreover, a normalization of the integrated areas to the gold content, taking in account the absorption coefficient, is needed to evaluate the relative contribution of the different gold sites in the three catalysts, because Au nanoparticles and Au clusters have different absorption coefficient, as shown in a recent paper [52,53]: on the basis of spectroscopic experiments of adsorbed CO and CO quantitative volumetric measurements, some of us have determined the absorption coefficients (cm^{-1} mol_{CO}^{-1} ($\times 10^4$)) equal to 3.2 as for Au nanoparticles and 1.3 for Au clusters. On the basis of these parameters, the total amount of exposed Au sites, expressed as mol_{CO}/mol_{Au}, in the three samples was calculated as the sum of clusters and nanoparticles, giving 0.274 for AuCe, 0.282 for AuCe80Zr20 and 0.408 for AuCe50Zr50. For the sake of clarity, the relative amounts of Au nanoparticles and Au clusters for the three catalysts are reported in the Table of the SI.

These data clearly show that AuCe50Zr50 has more uncoordinated gold sites than AuCe and AuCe80Zr20. The XRD analysis (see Fig. 1) showed that the Ce50Zr50 mixed support has a different crystalline structure, due to the presence of the solid solution. Despite of the involvement of Zr cations in the defective structures, the cubic-fluorite type structure of ceria is the predominant phase on AuCe80Zr20. These findings show that the Au dispersion and the consequent amount of Au sites can be strictly connected to the support structure.

Hence, a first possible explanation of the highest activity of AuCe50Zr50 displayed in the WGS reaction in the low temperature range (see Fig. 4) is the highest amount of uncoordinated gold sites. This observation is in agreement with very recent findings in which a correlation of the activity of differently prepared Au–$CeZrO_4$ catalysts with the surface concentration of adsorbed CO on the gold sites has been observed [54]. The experimental approach used in that paper involved the evaluation of the DRIFT Au–CO band area as a measure of the relative number of available active sites for the WGS reaction. In our case, these sites can be possibly related to the nucleation of gold on the mixed ceria–zirconia phase.

3.3.2. CO adsorbed at 120 K on the catalysts after WGS reaction

Adsorption of CO at 120 K was performed on the AuCe and AuCe50Zr50 catalysts after WGS reaction with aim to have further information on the different catalytic activity displayed in the WGS reaction, confirming the role of the uncoordinated gold sites and to explain stability and lack of deactivation shown by the AuCe50Zr50 catalyst (see Fig. 5).

In particular, the reaction was carried out on the samples previously reduced at 373 K in H_2, following the procedure: (1) inlet of the H_2O:CO mixture (3:1) at r.t.; (2) heating up to 623 K for 1 h in contact with the mixture; (3) cooling down to r.t. in the same mixture; (4) outgassing at r.t. to remove the WGS mixture. This procedure was chosen in order to mimic the operative conditions of the catalytic tests. Moreover, the same FTIR experiment was undertaken heating the samples in the WGS mixture up to 453 K, i.e. the temperature at which the difference between the catalytic activities of the mixed catalysts and AuCe is particularly evident (see Fig. 4). The results are not shown here because they are almost identical to those obtained heating the sample up to 623 K.

The FTIR spectra of CO adsorbed at 120 K on AuCe and AuCe50Zr50 samples after WGS reaction are reported in Fig. 6 (section a and b respectively, red curves).

First of all, the spectra of AuCe sample after WGS reaction are remarkably different from those collected before the reaction. In particular, the band at 2156 cm^{-1} disappeared, while a new band at 2150 cm^{-1}, associated to the low temperature interaction of CO molecules with OH surface groups, is evident. These features can be related to the simultaneous appearance of a huge absorption in the 1900–800 cm^{-1} range (not shown), due to the formation of carbonate/bicarbonate species during the WGS reaction. These species cover the support sites and inhibit the CO adsorption. Interestingly, the band at 2140 cm^{-1}, associated to the Ce^{3+}–CO interaction disappears and a peak at 2168 cm^{-1} increases contemporaneously. This frequency is congruent with the interaction between CO molecules and uncoordinated Ce^{4+} sites, meaning that a re-oxidation of the support sites occurred during the reaction. This hypothesis is also confirmed looking at the carbonylic bands due to Au species on AuCe (Fig. 6, section a, red line). In particular, an increase of the 2097 cm^{-1} band, associated to CO adsorbed on Au nanoparticles, occurs and at the same time an erosion of the component at low frequency is evident after WGS reaction. The erosion of the 2060–2040 cm^{-1} component is an indication that the Au clusters are no longer negatively charged. In fact, no charge transfer from the reduced support to the clusters can occur since ceria is re-oxidised. The simultaneous increase of the band at 2097 cm^{-1} confirms the presence of rounded gold nanoparticles that had flattened shape before the reaction, due to the strong interaction with reduced ceria. This structural change of the Au particles after WGS reaction has been proposed by Goguet et al. [40].

The WGS reaction mechanism is still matter of debate and, actually, two main reaction mechanisms have been proposed [1]. One is a redox mechanism [55,56] that involves the re-oxidation of the support, the other is an associative mechanism [57], where the main reaction intermediates are carbonate-like species. In

Table 1
Integrated areas of the carbonylic bands related to the gold before and after WGS reaction and relative amount of sites lost during reaction for AuCe and AuCe50Zr50.

Sample	Au[a] sites before WGS reaction	Au[a] sites after WGS reaction	Loss of Au[a] sites
AuCe	0.274	0.205	25%
AuCe50Zr50	0.408	0.258	37%

[a] Au nanoparticles + Au clusters (mol_{CO}/mol_{Au}).

his review on the WGS reaction, Burch has evidenced that the dominant mechanism depends on the on the reaction conditions, proposing an "universal" mechanism [1]. In our experimental conditions we firstly observe a re-oxidation of the catalysts accompanied by the formation of carbonate-like species (data not shown). Therefore, the indication of a specific mechanism would be speculative.

In the case of AuCe50Zr50 (Fig. 6, section b, red curve), the presence of a band in the 2100–2000 cm^{-1} range, due to Au–CO interaction, suggests that the behavior of the gold species after WGS reaction is comparable to that observed for AuCe. Interestingly, no frequency change in the position of the peaks due to CO adsorbed on support sites, i.e. 2158 and 2143 cm^{-1}, is evident on AuCe50Zr50 after reaction. In particular, only a decrease in intensity of the bands occurred.

The normalized integrated area of the carbonylic bands related to the gold sites has been evaluated before and after WGS reaction for both samples and the results have been reported in Table 1 together with the relative amount of sites lost during reaction. More in detail, the integrated areas of the bands due to the Au–CO interaction after WGS reaction have been normalized to the gold content, taking into account the absorption coefficient as reported previously.

According to Ref. [54], the high activity of AuCe50Zr50 can be directly related to the amount of Au sites, that is higher than on AuCe. Unexpectedly, the most active and stable AuCe50Zr50 catalyst loses the highest amount of uncoordinated gold sites after reaction. This feature should be accompanied by a significant deactivation observed on repeating the temperature ramp [39]. However, the catalytic performance of AuCe50Zr50 is almost the same if comparing the I run with the II one (see Fig. 5). On this basis, it is very hard to explain the stability displayed by our catalyst, if only the total amount of gold sites is taken in account.

The integrated areas of the bands related to CO interaction with support sites were also calculated and they are listed in Table 2. In this case only the comparison between the situation before and after the WGS reaction for each sample has been done without preliminar normalization.

The comparison between the number of support sites available by the two catalysts after WGS reaction shows that AuCe loses 33% of the sites during the reaction against 18% lost by AuCe50Zr50, indicating that some blockage of the support sites by carbonate-like species formed during the WGS reaction occurred [36]. Moreover, the decomposition of these adsorbed species is more efficient on AuCe50Zr50 than on AuCe, in agreement with the high stability shown by the AuCe50Zr50 catalyst.

Table 2
Integrated areas of the carbonylic bands related to support sites before and after WGS reaction and relative amount of sites lost during reaction for AuCe and AuCe50Zr50.

Sample	Support sites before WGSR	Support sites after WGSR	Loss of support sites
AuCe	20.319	13.517	33%
AuCe50Zr50	25.566	20.740	18%

This feature can be connected to the changes in the surface properties of ceria induced by the addition of zirconia. In fact, it is well known that doping the lattice of ceria enhances the reducibility and thermal resistance of ceria [58]. Beside the modification of the redox properties, the addition of zirconia can change the acid/base properties of a basic surface oxide like CeO_2. As a consequence the adsorption of carbonate-like species is less favored, as well as their stability can be lower.

3.3.3. Characterization of the supports by acetone

The acid–base properties of the supports can be investigated by in situ FTIR spectroscopy of small adsorbed basic molecules [59]. Normally NH_3, pyridine, CH_3CN, NO or CO molecules, have been used for characterizing the nature, the strength and the concentration of acid sites. Zaki et al. [60] have successfully employed an in situ IR study of adsorbed acetone to investigate the acid–base properties of metal oxide surfaces. The authors have reported that acetone molecules are firstly irreversibly adsorbed via coordination to Lewis acid sites ($(CH_3)_2C{=}O \rightarrow M^{n+}$); then the acetone ligands may be activated for α-hydrogen abstraction resulting in the formation of anionic enolate type ions ($CH_2(CH_3)C{-}O^- \rightarrow M^{n+}$), and successively, an aldol-condensation-type of surface reaction may occur. The anionic enolate type ions and condensed species, as DAA, diacetone alcohol ($((CH_3)_2C(OH){-}CH_2(CH_3)C{=}O \rightarrow M^{n+}$) and MSO, mesytil oxide ($((CH_3)_2C{=}CH{-}(CH_3)C{=}O \rightarrow M^{n+}$) species are formed, provided that the coordination site is strongly acidic and has a basic site (surface $-OH^-$ or $-O^{2-}$ site) in close proximity. Moreover, the C=O stretching frequency of these species falls in different ranges, i.e. 1720–1650 cm^{-1} for acetone and 1650–1550 cm^{-1} for condensed species, so it is possible to monitor their formation and their abundance using in situ IR spectroscopy. Zaki et al. [60] have demonstrated that for an acid oxide, as zirconia, the adsorbed acetone molecules are more abundant than the condensed species, on the contrary, for a basic oxide, as ceria, the condensed species are prevalent. Hence, from the relative amounts of these adsorbed species it is possible to evaluate the acid/base properties of the oxides. With this aim, FTIR measurements of adsorbed acetone at r.t. on the three bare oxide supports, i.e. CeO_2, Ce50Zr50 and Ce80Zr20, have been undertaken. The samples have been previously submitted to a thermal treatment at 673 K in oxygen, in order to clean the surface. Moreover, in order to exclude that the deposition of gold on the supports could modify the surface of the oxides, the same experiment has been performed on the AuCe50Zr50 sample (not shown for the sake of brevity). The results evidenced that the deposition of gold does not change the nature of surface support sites.

In Fig. 7 the spectra collected after interaction with acetone at r.t. (10 min) of CeO_2 (section a), Ce50Zr50 (section b) and Ce80Zr20 (section c) are reported. To evaluate the contribution of the different adsorbed species, a careful deconvolution of the complex absorption bands (Fig. 7) of adsorbed acetone and condensed species has been carried out and the integration of the extrapolated bands (Fig. 7, dashed lines) has been done. The obtained integrated areas are summarized in Table 3; also in this case the normalization is not required.

Interestingly, molecular acetone is the predominant adsorbed species on the mixed oxides, whilst on ceria the condensed species are slightly more abundant. This result highlights that the addition of zirconia to ceria makes the mixed oxides more acid than pure CeO_2.

In particular, the ratio between the integrated area of molecular acetone and condensed species is equal to 0.8 for ceria, 1.6 for Ce50Zr50 and 1.5 for Ce80Zr20, evidencing that the addition of different amounts of ZrO_2 to ceria gives rise to the same acid/base properties (the acidity of the two mixed oxides is quite similar).

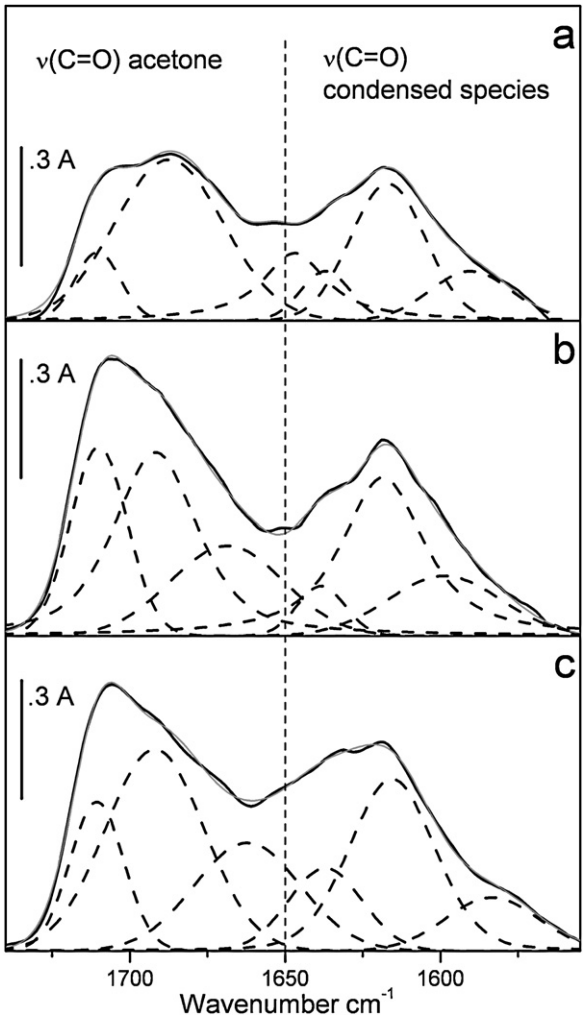

Fig. 7. FTIR spectra of CeO_2 (black line, section a), Ce50Zr50 (black line, section b) and Ce80Zr80 (black line, section c) collected after acetone adsorption at r.t. Curvefit and extrapolated bands (dashed lines) are reported.

Moreover, basing on the calculated ratio, the acidity of the two mixed oxides is two times higher than that of ceria. It is well known that carbonate/formate species, responsible for the deactivation of the catalyst are strongly adsorbed on the surface of a basic oxide like CeO_2; therefore the increase of the acidity by the addition of zirconia can lower the stability of these species.

A more efficient decomposition of the adsorbed species on the mixed oxide catalysts than on AuCe sample can also explain the catalytic stability of AuCe50Zr50, in agreement with the FTIR data previously discussed and supporting the high activity of this sample. For the same reasons also the other mixed oxide catalyst AuCe80Zr20 performs better than AuCe. But, considering the similar acidity of the two mixed supports, the different catalytic activity between AuCe50r50 and AuCe80Zr20 makes sense only taking in account also their different Au dispersion: as evidenced by HRTEM and FTIR, AuCe80Zr20 displays Au particles larger than those observed on AuCe50Zr50.

Table 3
Integrated areas of the bands obtained after acetone adsorption at r.t.

Sample	Peaks area[a], 1720–1650 cm^{-1} range	Peaks area[b], 1650–1550 cm^{-1} range
CeO_2	20.329	23.925
Ce50Zr50	38.496	24.230
Ce80Zr20	40.217	26.979

[a] (Ac → cation sites).
[b] (Cond → cation sites).

4. Conclusion

HRTEM analysis and FTIR measurements showed that the addition of another oxide (ZrO_2) to ceria leads to different Au dispersion, depending also on the zirconia amount. In particular, the combined use of these techniques allowed evidencing the presence of two different gold species on the surface of the studied samples, i.e. Au nanoparticle sites and Au cluster sites. More in detail, HRTEM measurements showed the presence of Au agglomerates (10–20 nm) and nanoparticles (about 2.5 nm) on AuCe80Zr20, while on AuCe50Zr50 only gold nanoparticles are observed. At the same time, FTIR spectroscopy of adsorbed CO indicates that there are also Au clusters (not detectable by HRTEM) and that their amount is higher on AuCe50Zr50 than on AuCe80Zr20. Furthermore, the integrated areas of the bands due to Au–CO interaction have well evidenced that AuCe50Zr50 has the highest amount of uncoordinated Au sites, higher than that on AuCe and AuCe80Zr20. These features can be strictly connected to the oxide structure, that by XRD has been shown to be totally a ceria–zirconia solid solution only in the case of the support of AuCe50Zr50.

The FTIR measurements also revealed that the addition of zirconia modifies the acid/base properties of the mixed oxides. In particular, different amounts of ZrO_2 added to ceria gives rise to quite similar acidity of Ce50Zr50 and Ce80Zr20. In both cases, the acidity is two times higher than that of ceria. Moreover, the WGS activity of the gold catalysts at low temperature is influenced by the addition of zirconia, too. In fact, both catalysts on mixed oxide supports show better performance in the low-temperature WGS reaction respect to AuCe, according to the following trend: AuCe50Zr50 > AuCe80Zr20 > AuCe. Therefore, the very good catalytic activity of AuCe50Zr50 is correlated not only to the abundance of gold clusters and nanoparticles, but also to the effect of ZrO_2, that lowers the basicity respect to the pure ceria. Adsorption and surface reaction of acetone vapor at room temperature have been successfully employed for dosing this last effect.

Therefore, the comparison of the integrated areas of the CO bands on the support sites before and after WGS reaction clearly demonstrated that the carbonate-like species have low stability on the AuCe50Zr50 surface. This feature, along with the presence of a high gold dispersion, makes AuCe50Zr50 the best catalyst in terms of catalytic activity and stability. The results obtained on AuCe80Zr20 evidenced that the acid/base properties are not enough to make this catalyst active in the WGS reaction as well as AuCe50Zr50, because high Au dispersion is also needed.

Acknowledgements

F.V., M.M., F.B. and A.C. gratefully acknowledge the financial support by Istituto Italiano di Tecnologia (IIT) Genova, Italy. T.T. and V.I. gratefully acknowledge the financial support by the Bulgarian National Science Fund (Project DDVU 02/7).

Appendix A. Supplementary data

Supplementary data associated with this article can be found, in the online version, at http://dx.doi.org/10.1016/j.apcatb.2012.05.031.

References

[1] R. Burch, Physical Chemistry Chemical Physics 8 (2006) 5483–5500.
[2] M.S. Chen, D.W. Goodman, Catalysis Today 111 (2006) 22–33.
[3] F. Boccuzzi, A. Chiorino, M. Manzoli, D. Andreeva, T. Tabakova, L. Ilieva, V. Iadakiev, Catalysis Today 75 (2002) 169–175.

[4] V. Idakiev, T. Tabakova, Z.Y. Yuan, B.L. Su, Applied Catalysis A-General 270 (2004) 135–141.
[5] V. Idakiev, Z.Y. Yuan, T. Tabakova, B.L. Su, Applied Catalysis A-General 281 (2005) 149–155.
[6] V. Idakiev, T. Tabakova, A. Naydenov, Z.Y. Yuan, B.L. Su, Applied Catalysis B: Environmental 63 (2006) 178–186.
[7] T. Tabakova, V. Idakiev, K. Tenchev, F. Boccuzzi, M. Manzoli, A. Chiorino, Applied Catalysis B: Environmental 63 (2006) 94–103.
[8] T. Tabakova, M. Manzoli, D. Paneva, F. Boccuzzi, V. Idakiev, I. Mitov, Applied Catalysis B: Environmental 101 (2011) 266–274.
[9] A. Luengnaruemitchai, S. Osuwan, E. Gulari, Catalysis Communications 4 (2003) 215–221.
[10] E.V. Rebrov, A. Berenguer-Murcia, B.F.G. Johnson, J.C. Schouten, Catalysis Today 138 (2008) 210–215.
[11] J. Li, N. Ta, W. Song, E. Zhan, W. Shen, Gold Bulletin 42 (2009) 48–60.
[12] J. Li, J. Chen, W. Song, J. Liu, W. Shen, Applied Catalysis A-General 334 (2008) 321–329.
[13] Z. Ma, H. Yin, S. Dai, Catalysis Letters 136 (2010) 83–91.
[14] M. Boaro, M. Vicario, J. Llorca, C. de Leitenburg, G. Dolcetti, A. Trovarelli, Applied Catalysis B: Environmental 88 (2009) 272–282.
[15] F. Zane, V. Trevisan, F. Pinna, M. Signoretto, F. Menegazzo, Applied Catalysis B: Environmental 89 (2009) 303–308.
[16] A. Sandoval, A. Gomez-Cortes, R. Zanella, G. Diaz, J.M. Saniger, Journal of Molecular Catalysis A: Chemical 278 (2007) 200–208.
[17] M. Shekhar, J. Wang, W.S. Lee, W.D. Williams, S.M. Kim, E.A. Stach, J.T. Miller, W.N. Delgass, F.H. Ribeiro, Journal of the American Chemical Society 134 (2012) 4700–4708.
[18] Q. Fu, A. Weber, M. Flytzani-Stephanopoulos, Catalysis Letters 77 (2001) 87–95.
[19] D. Andreeva, V. Idakiev, T. Tabakova, L. Ilieva, P. Falaras, A. Bourlinos, A. Travlos, Catalysis Today 72 (2002) 51–57.
[20] Q. Fu, H. Saltsburg, M. Flytzani-Stephanopoulos, Science 301 (2003) 935–938.
[21] G. Jacobs, S. Ricote, P.M. Patterson, U.M. Graham, A. Dozier, S. Khalid, E. Rhodus, B.H. Davis, Applied Catalysis A-General 292 (2005) 229–243.
[22] H. Sakurai, T. Akita, S. Tsubota, M. Kiuchi, M. Haruta, Applied Catalysis A-General 291 (2005) 179–187.
[23] C. Galletti, S. Specchia, G. Saracco, V. Specchia, Topics in Catalysis 52 (2009) 688–692.
[24] B.S. Caglayan, A.E. Aksoylu, Catalysis Communications 12 (2011) 1206–1211.
[25] R. Leppelt, B. Schumacher, V. Plzak, M. Kinne, R.J. Behm, Journal of Catalysis 244 (2006) 137–152.
[26] Y. Denkwitz, A. Karpenko, V. Plzak, R. Leppelt, B. Schumacher, R.J. Behm, Journal of Catalysis 246 (2007) 74–90.
[27] A. Karpenko, R. Leppelt, V. Plzak, J. Cai, A. Chuvilin, B. Schumacher, U. Kaiser, R.J. Behm, Topics in Catalysis 44 (2007) 183–198.
[28] A. Karpenko, R. Leppelt, J. Cai, V. Plzak, A. Chuvilin, U. Kaiser, R.J. Behm, Journal of Catalysis 250 (2007) 139–150.
[29] A. Karpenko, R. Leppelt, V. Plzak, R.J. Behm, Journal of Catalysis 252 (2007) 231–242.
[30] A.A. El-Moemen, G. Kucerova, R.J. Behm, Applied Catalysis B: Environmental 95 (2010) 57–70.
[31] A. Trovarelli, C. de Leitenburg, G. Dolcetti, Chemtech 27 (1997) 32–37.
[32] A. Trovarelli, in: A. Trovarelli (Ed.), Catalysis by Ceria and Related Materials, Imperial College Press, London, 2002, pp. 15–50.
[33] J. Kaspar, P. Fornasiero, in: A. Trovarelli (Ed.), Catalysis by Ceria and Related Materials, Imperial College Press, London, 2002, pp. 217–242.
[34] S.J. Schmieg, D.N. Belton, Applied Catalysis B: Environmental 6 (1995) 127–144.
[35] R. Di Monte, P. Fornasiero, J. Kaspar, M. Graziani, J.M. Gatica, S. Bernal, A. Gomez-Herrero, Chemical Communications (2000) 2167–2168.
[36] C.H. Kim, L.T. Thompson, Journal of Catalysis 230 (2005) 66–74.
[37] C.H. Kim, L.T. Thompson, Role of Zirconia in Stabilyzing Ceria Supported Gold Water Gas Shift Catalysts, "GOLD 2006" New Industrial Application for Gold, Limerick, Ireland, 2006, p. 57.
[38] D. Duprez, C. Descrome, in: A. Trovarelli (Ed.), Catalysis by Ceria and Related Materials, Imperial College Press, London, 2002, pp. 243–280.
[39] D. Tibiletti, A. Amieiro-Fonseca, R. Burch, Y. Chen, J.M. Fisher, A. Goguet, C. Hardacre, P. Hu, A. Thompsett, Journal of Physical Chemistry B 109 (2005) 22553–22559.
[40] A. Goguet, R. Burch, Y. Chen, C. Hardacre, P. Hu, R.W. Joyner, F.C. Meunier, B.S. Mun, A. Thompsett, D. Tibiletti, Journal of Physical Chemistry C 111 (2007) 16927–16933.
[41] M. Yashima, H. Takashina, M. Kakihana, M. Yoshimura, Journal of the American Ceramic Society 77 (1994) 1869–1874.
[42] M. Yashima, H. Arashi, M. Kakihana, M. Yoshimura, Journal of the American Ceramic Society 77 (1994) 1067–1071.
[43] T. Tabakova, F. Boccuzzi, M. Manzoli, D. Andreeva, Applied Catalysis A-General 252 (2003) 385–397.
[44] R. Di Monte, J. Kaspar, Journal of Materials Chemistry 15 (2005) 633–648.
[45] C. Binet, M. Daturi, J.C. Lavalley, Catalysis Today 50 (1999) 207–225.
[46] M. Daturi, C. Binet, J.C. Lavalley, G. Blanchard, Surface and Interface Analysis 30 (2000) 273–277.
[47] D.W. Goodman, Catalysis Letters 99 (2005) 1–4.
[48] M.S. Chen, D.W. Goodman, Science 306 (2004) 252–255.
[49] F. Vindigni, M. Manzoli, A. Chiorino, F. Boccuzzi, Gold Bulletin 42 (2009) 106–112.
[50] T. Akita, M. Okumura, K. Tanaka, M. Kohyama, M. Haruta, Catalysis Today 117 (2006) 62–68.
[51] M. Manzoli, F. Boccuzzi, A. Chiorino, F. Vindigni, W. Deng, M. Flytzani-Stephanopoulos, Journal of Catalysis 245 (2007) 308–315.
[52] A. Chiorino, M. Manzoli, F. Menegazzo, M. Signoretto, F. Vindigni, F. Pinna, F. Boccuzzi, Journal of Catalysis 262 (2009) 169–176.
[53] F. Menegazzo, F. Pinna, M. Signoretto, V. Trevisan, F. Boccuzzi, A. Chiorino, M. Manzoli, Applied Catalysis A-General 356 (2009) 31–35.
[54] R. Pilasombat, H. Daly, A. Goguet, J.P. Breen, R. Burch, C. Hardacre, D. Thompsett, Catalysis Today 180 (2012) 131–138.
[55] K. Li, Q. Fu, M. Flytzani-Slephanopoulos, Applied Catalysis B: Environmental 27 (2000) 179–191.
[56] F. Boccuzzi, A. Chiorino, M. Manzoli, D. Andreeva, T. Tabakova, Journal of Catalysis 188 (1999) 176–185.
[57] F.C. Meunier, D. Tibiletti, A. Goguet, S. Shekhtman, C. Hardacre, R. Burch, Catalysis Today 126 (2007) 143–147.
[58] M. Vicario, J. Llorca, M. Boaro, C. de Leitenburg, A. Trovarelli, Journal of Rare Earths 27 (2009) 196–203.
[59] M.I. Zaki, M.A. Hasan, F.A. Al-Sagheer, L. Pasupulety, Colloids and Surfaces A: Physicochemical and Engineering Aspects 190 (2001) 261–274.
[60] M.I. Zaki, M.A. Hasan, L. Pasupulety, Langmuir 17 (2001) 768–774.